KSME International Journal, Vol. 14, No. 8, pp. 867~878, 2000

Unsteady Aerodynamic Loads on High Speed Trains Passing by Each Other

Jaeho Hwang*

Research Assistant, Department of Aerospace Engineering, Institute of Advanced Machinery Design, Seoul National University

Dong-Ho Lee

Professor, School of Mechanical and Aerospace Engineering, Seoul National University

In order to study unsteady aerodynamic loads on high speed trains passing by each other 350km/h, three-dimensional flow fields around trains during the crossing event are numerically simulated using three-dimensional Euler equations. Roe's FDS with MUSCL interpolation is employed to simulate wave phenomena. An efficient moving grid system based on domain decomposition techniques is developed to analyze the unsteady flow field induced by the restricted motion of a train on a rail. Numerical simulations of the trains passing by on the double-track are carried out to study the effect of the train nose-shape, length and the existence of a tunnel on the crossing event. Unsteady aerodynamic loads-a side force and a drag force -acting on the train during the crossing are numerically predicted and analyzed. The side force mainly depends on the nose-shape, and the drag force depends on tunnel existence. Also. a push -pull (i.e.impluse force) force successively acts on each car and acts in different directions between the neighborhood cars. The maximum change of the impulsive force reaches about 3 tons. These aerodynamic force data are absolutely necessary to evaluate the stability of high speed multi-car trains. The results also indicate the effectiveness of the present numerical method for simulating the unsteady flow fields induced by bodies in relative motion.

Key Words : High Speed Train, Crossing, Domain Decomposition Technique

Nomenclature

A, B, C	: Inviscid flux Jacobian
C_s	: Side force coefficient
C_d	: Drag coefficient
C_l	: Lift coeffient
D	: Tunnel diameter or diagonal matrix
E	: Total energy
E, F, G	: Inviscid flux vector
FDS	: Flux Difference Splitting
FSA	: Fortified Solution Algorithm
GLS	: Galerkin Least Squares
I	: Identity matirx
J	: Jacobian of transformation
$MUSCL$	: Monotone Upstream-Centered Scheme for Conservation Law
P	: Pressure
Q	: Vector of conservative variables
u, v, w	: Velocity vector
x, y, z	: Cartesian coordinate

Greek

γ	: Specific heat
ρ	: Density
ξ, η, ζ	: Generalized coordinate

* Corresponding Auther,
E-mail : aeroj@bigfoot.com
TEL : +82-2-880-8051; **FAX** : +82-2-889-6205
Research Assistant, Department of Aerospace Engineering, Institute of Advonced Machinery Design, Seoul National University, San 56-1, Shinlim-dong, Kwanak-Ku, Seoul 151-742, Korea.(Manuscript **Received** November 12, 1999; **Revised** June 3, 2000)

1. Introduction

The increased speed of a high speed train (e. g a magnetic levitation vehicle) generates many aer

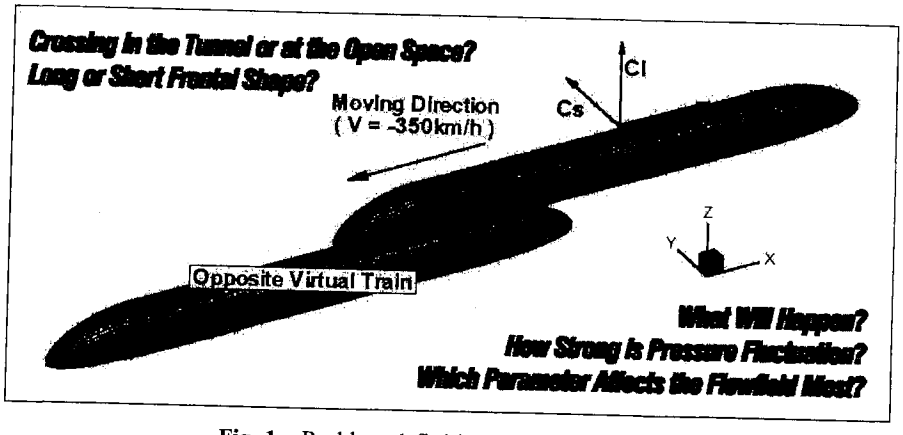

Fig. 1 Problem definition of crossing Trains

odynamic problems (Peters, 1981), especially when going through tunnels or passing each other.

When two trains pass each other, at 350km/m 3-dimensional unsteady impulsive aerodynamic loads may destabilize the trains, leading to unfavorable snake-like motions by push-pull like side force. Also, large pressure fluctuation over the trains would be expected during the crossing event. Therefore, to enhance passenger comfort and stability, better understanding of the unsteady flow phenomena induced by the trains is required. However, the flow details and unsteady aerodynamic forces during the crossing event are not yet well understood as shown in Fig. 1.

Kim(1997) adopted a 1-dimensional characteristic approach and showed good results for 1-dimensional pressure variations in the tunnel. However, the crossing event is essentially a 3-dimensional phenomenon. Therefore the 1 -dimensional approach is inadequate for the 3 -dimensional efferts such as the side force and yawing moment. Fujii and Ogawa (1995) computed a three-dimensional flow induced by two trains passing each other inside a tunnel using FSA (Fujii, 1992). Though Fujii's approach reveals the basic nature of the crossing event, his approach is not applicable to the other crossing cases because of the computational inefficiency in grid topology. There are many unknown parameters on the crossing event including the nose shape, crossing location, train length and gap between the trains. Therefore, a more problem -oriented efficient grid system and solution strategy are needed.

In the present study, a 3-dimensional compressible, inviscid code is developed to analyze the flow field around high speed trains in relative motion in open space and in tunnels. Since the viscous effects on the wave characteristics are negligibly small as shown by Maeda (1993), and since we focus on the global flow characteristics to study the force coefficients, an inviscid calculation would be sufficient. A higher order Roe's upwind scheme with MUSCL and van Albada limiter function is employed to simulate the pressure wave phenomena-generation at the entrance, propagation through the tunnel, reflection at the end of the tunnel and interaction again with the trains. A smart moving grid technique based on domain decomposition technique is applied to analyze the unsteady flow field induced by the restricted motion of a train on a rail. Due to the restricted linear motion of trains, the grid system can be tuned up without losing generality; consequently, less computational resources are needed as suggested by Hwang and Lee (1998, 1999). The code was validated through a comparison with single track experimental values from Kwon et al. (1998)

The numerical simulations of trains passing at 350 km/h are carried out for 2 nose-shapes each other. The configuration of the KHST (Korean High Speed Train) under development are used. The crossing flow phenomena are studied for the trains passing by outside and inside a tunnel.

And, finally the number of cars is changed to examine the length effect and side force variation -push-pull like side force - on each car. So, a parametric study on the flow field around trains passing by each other is performed to understand basic nature of the crossing event.

This paper is organized as follows. In Sec. 2, the current numerical procedure is introduced briefly, including a unique problem-oriented grid strategy. In Sec. 3, the test cases are defined and after validation of the current method, the computed results are discussed. Finally, concluding remarks are drawn.

2. Numerical Procedure

2.1 Governing equations

We focus on the unsteady, compressible, three-dimensional Euler equations. In physical coordinates, the equations are

$$\frac{\partial Q}{\partial t}+\frac{\partial E}{\partial x}+\frac{\partial F}{\partial y}+\frac{\partial G}{\partial z}=0, \tag{1}$$

where

$$Q=\begin{pmatrix}\rho\\ \rho u\\ \rho v\\ \rho w\\ \rho e\end{pmatrix},\ E=\begin{pmatrix}\rho u\\ \rho u^2+P\\ \rho uv\\ \rho uw\\ (\rho e+P)u\end{pmatrix},$$

$$F=\begin{pmatrix}\rho u\\ \rho uv\\ \rho v^2+P\\ \rho vw\\ (\rho e+P)v\end{pmatrix},\ G=\begin{pmatrix}\rho w\\ \rho uw\\ \rho vw\\ \rho w^2+p\\ (\rho e+P)w\end{pmatrix},$$

and the equation of state yields

$$e=\frac{1}{\rho(\gamma-1)}P+\frac{1}{2}(u^2+v^2+w^2) \tag{2}$$

where the ratio of specific heats γ is 1.4.

2.2 Numerical discretization

2.2.1 Space discretization

Roe's finite volume flux difference splitting technique (Roe, 1981) is used for spatial discretization and MUSCL with van Albada flux limiter function is used to achieve a high order of spatial accuracy. The present computation has a third-order spatial accuracy. The Roe's numerical flux at the cell interface can be expressed as Eq. (3).

$$\hat{E}(Q_L, Q_R)=\frac{1}{2}[\hat{E}(Q_R)+\hat{E}(Q_L) - |\hat{A}(Q_L, Q_R)|(Q_L-Q_R)] \tag{3}$$

where,

$$\hat{A}(Q_L, Q_R)=\frac{\partial\hat{E}(Q)}{\partial Q}$$

2.2.2 Time integration

Calculations of unsteady, three-dimensional flow field around moving body require a time accurate numerical scheme and huge computational resources. In the present study, Yoon's LU-SGS scheme (Yoon, 1987) is chosen for efficient time integration. The factorized form of the governing equation is

$$(LD^{-1}U)\Delta Q=-R, \tag{4}$$

where

$$L=\frac{I}{J\Delta t}+D_\xi^-A^+ +D_\eta^-B^+ +D_\zeta^-C^+ -A^- -B^- -C^-,$$

$$D=\frac{I}{J\Delta t}+A^+ -A^- +B^+ -B^- +C^+ -C^-,$$

$$U=\frac{I}{J\Delta t}+D_\xi^+A^- +D_\eta^+B^- +D_\zeta^+C^- +A^+ +B^+ +C^+,$$

2.3 Grid system

The grid system for computing three dimensional train/tunnel interaction and train/train interaction is characterized by a moving body confined to linear motions on the rail, relative motions between solid bodies, ground proximity and long tunnels. So, it takes huge computational resources with conventional grid systems such as Chimera grid (Steger et al., 1983) and unstructured mesh (Mestreau, 1993), both in time and storage device.

To accommodate the relative motion, Fujii(1995) and Ogawa(1994, 1997) used FSA (Fortified Solution Algorithm) (Fujii, 1992), and they successfully computed the tunnel entry and crossing problems. Fujii's approach is similar to the Chimera procedure (Steger et al., 1983)-com-

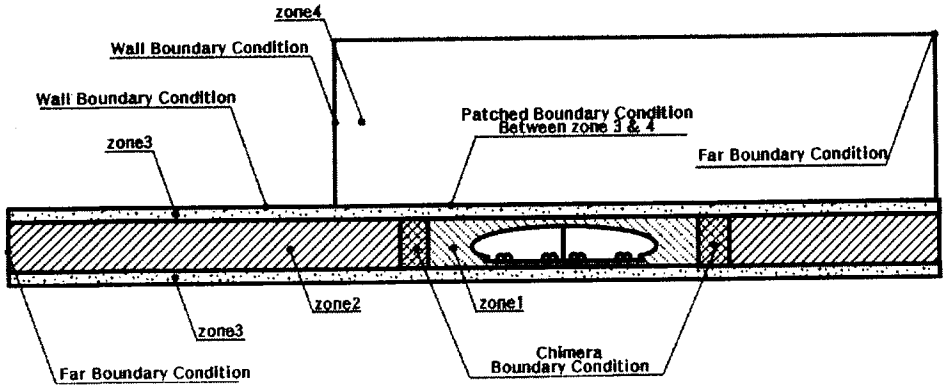

Fig. 2 Schematic diagram of zonal interface using 3 types of domain decomposition technique

posed of hole construction and linear interpolation at boundaries, so a strict criteria on boundaries such as moderate cell volume ratio between giving cell and target cell is necessary to get a stable solution. If the region to be swept by the train is large, there should be a large number of grid points along the region to satisfy proper interpolation criterion through the whole 3-dimensional computational domain. Fujii and Ogawa(1997) used an intermediate zone to overcome this requirement, but it makes the computation inefficient because the intermediate zone requires more linear interpolation routines.

As an alternative, Mestreau(1993) used an unstructured grid with automatic remeshing and Holmes(1999) applie moving boundary condition to the tunnel wall, using a flow solver based on GLS finite element formulation. These grid systems can be applied to limited cases(e. g. tunnel entry problem), and they are not suitable for parametric studies using several parameters because of costly remeshing and sophisticated assumptions on the grid system.

Hwang and Lee(1998, 1999) suggested that the grid system could be tuned up to avoid costly unsteady remeshing and sophisticated assumptions by choosing of domain decomposition technique carefully.

In the present study, 3 types of domain decomposition techniques-multi-block grid, patched grid, and overlapping grid-are applied. Figure 2 shows a schematic diagram of a smart grid system and the zonal interface for the tunnel entry problem. The grid system can be extended to train/train crossing and tunnel outgoing problems just by imposing line symmetric boundary condition and adding an extra computational domain at the exit region. Zone 1 is a moving zone around a high speed train, and Zone 2 is a background zone which overlaps with Zone 1. Consequently, a simplified Chimera hole construction and linear interpolation routines between Zone 1 and 2 are needed only at the fore and aft parts of Zone 1. Compared with the 3-dimensional Chimera procedures, the current method is more efficient because it uses much fewer fringe cells and do not uses additional iterations to find interpolation coefficients. Considering the mild variation of the flow variables except the in vicinity of the train and 1-dimensional wave phenomena in the tunnel, the linear interpolation can be used with great reliability, without adopting a tedious 3-dimensional conservative treatment of Rai (1986).

As an intermediate Zone, Zone 3 shares a sliding surface with Zone 1, and a conservative patching algorithm is applied at the surface. By using this intermediate zone, code can be extended for the crossing case. Zone 4 is the tunnel entrance zone. For computing the unsteady flow field around a train going into/out of a tunnel, simply adding Zone 5 at the other end of the tunnel is sufficient as shown in Fig. 3. Figure 4 shows a schematic of grid system for a computation of the crossing case. By generating the grid system on the half of the double track, and by applying a line symmetric boundary condition at

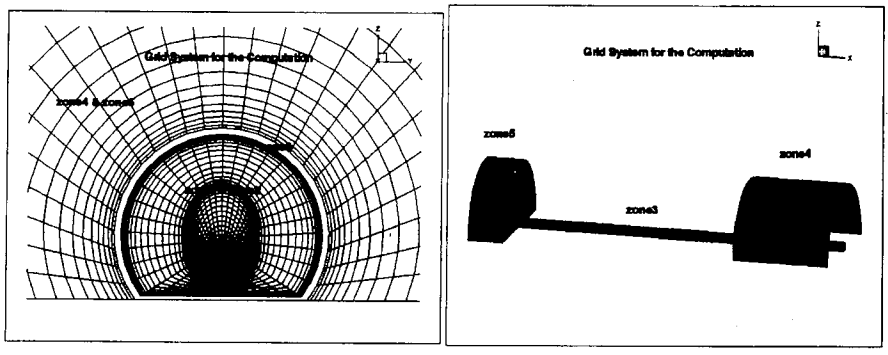

Fig. 3 Grid system for train running on single track (5 block zonal approach)

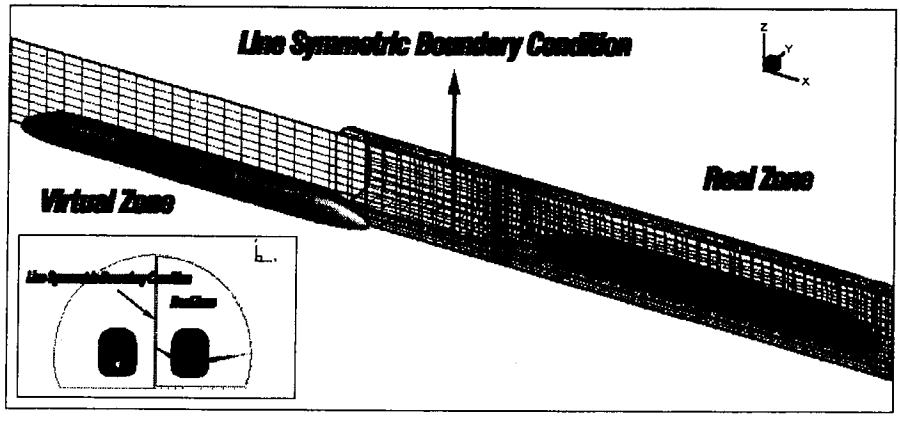

Fig. 4 Schematic diagram of grid system for the crossing case using line symmetric boundary condition

the symmetric surface on one intermediate zone, simulation of the crossing event on the double track can be realized without other changes.

3. Results and Discussions

For the present study deals with an aperiodic unsteady problem, the unsteady field data are stored during the whole computation. And, numerous field data are post-processed to time histories of force coefficient and to other various forms, including animations of unsteady flow field.

In the present computation, three reference times are used for convenience. Dealing with the whole process, time is set to zero when starting the computation. Concentrating on specific events, (e. g. the tunnel entrance and the crossing), time is set to zero when the nose enters the tunnel or when noses cross.

3.1 Code validation

To validate the code, a numerical result is compared with the experimental values from Kwon et al. (1998) for a tunnel entry problem. Experiment was performed at a train-tunnel test facility in NLR, Netherlands. The pressure probe is located at 4% from the tunnel entrance to defect a compression wave front. The train speed is 350km/h and the blockage ratio is 0.083. In Fig. 5, we can see that the numerical result matches well with the experimental values.

3.2 Trains on the double track

3.2.1 Problem definition

Due to the difficulties in studying on the crossing event of the high speed trains, only a few and limited numerical studies (Fujii, 1995) and exper imental researches (Shimbo, 1993) have been re-

Table 1 Definition of the Cases

Case	Shape of train	Crossing region	Train length
LFCT	Long frontal shape(15m long)	In the tunnel	40m(2 CAR)
SFCT	Short frontal shape(6.64m long)	In the tunnel	40m (2 CAR)
LFCO	Long frontal shape(15m long)	At the open space	40m (2 CAR)
SFCO	Short frontal shape(6.64m long)	At the open space	40m (2 CAR)
SFCO3	Short frontal shape(15m long)	At the open space	60m(3 CAR)

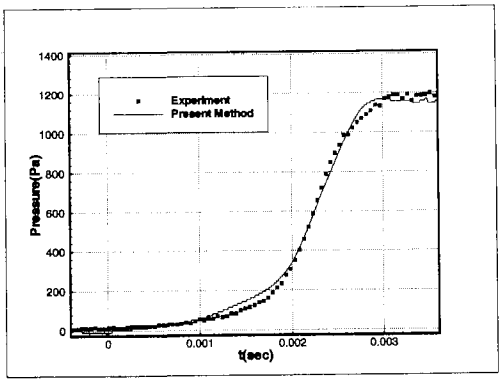

Fig. 5 Compression wave front generated by train running at 350km/h(Kwon et al. 1998)

ported. Shimbo(1993) measured only the pressure data at the limited points over train surface during the crossing event and reported asymmetric pressure distribution. But, parametric studies about the crossing event have not yet been done. Therefore, to understand the unsteady aerodynamic forces associated with crossing, 3 basic parameters-the nose shape (long and short frontal shapes), location (inside and ontside a tunnel) and train the length (train of 2 cars and 3 cars)-are selected for the current research. The shapes of train and tunnel are given by KHST, and they are simplified to facilitate grid generation. Since, we concentrate on the global flow physics, the shape of train is generated just to satisfy the frontal view(cross-section), the plan view, the side view and the area distribution along the nose. Table. 1 shows the definition of the adopted 5 cases.

The width, height and cross-sectional area of the train are 2.80 m, 3.50 m, and 9.00 m^2 respectively And the cross-sectional area of the tunnel is 108 m^2. The length of the train is set to 40 m,

Table 2 Number of grid points and initial distances

Case	No. of grid points	Initial distance between the trains
LFCT	341,941	48.60 D(about 457m)
SFCT	488,061	66.25 D(about 623m)
LFCO	235,471	21.14 D(about 199m)
SFCO	302,051	21.14 D(about 199m)
SFCO3	316,111	21.14 D(about 199m)

approximately twice the length of the power car except in the case SFCO3 of 60 m representing 3 cars. Table 2 lists the number of grid points used for each case and the initial position between the trains. The height of the tunnel D is chosen as a reference length. In the computations, the global time step, $\Delta t = 0.01$/iteration is used for all cases after the time step sensitivity study on the load histories. It takes 3.8×10^{-5} sec per grid point for 1 iteration with a 450Mhz Digital Alpha CPU and the interpolation time between the domains is less than 1% of the total time per one iteration. Figure 6 shows the frontal view of the grid system used for the case SFCT, and the grid length in x-direction could be shortened for the cases of crossing at the open space (LFCO, SFCO, SFCO3) by neglecting the tunnel region.

3.2.2 Aerodynamic force history

The spatial distribution of pressure along the tunnel wall during the crossing is shown in Fig. 7 for in SFCT case. The positions of pressure probes are given in Fig. 6, In Fig. 7, the reflected pressure waves at the open end of the tunnel are

shown. The figures also show that pressure field induced by a virtual opposite train is acceptably simulated by the line symmetric boundary condition. And, it can be clarified from the first figure of Fig. 7 that except in the vicinity of trains, the flow field in a tunnel is nearly 1-dimensional. During the crossing event, it is expected that the train may undergo complex aerodynamic load condition.

The definition of aerodynamic force coefficients-Cd(Drag Force), Cs(Side Force), Cl(Lift Force)-is given in Fig. 1. The time for load histories is set to zero when the trains start crossing, and accordingly t = 15.32 when the trains finish crossing. At t=7.66, the two trains are located exactly side by side. And the times are increased by factor of 1.5 when for the SFCO3 case due to the increased length of the train by the same factor.

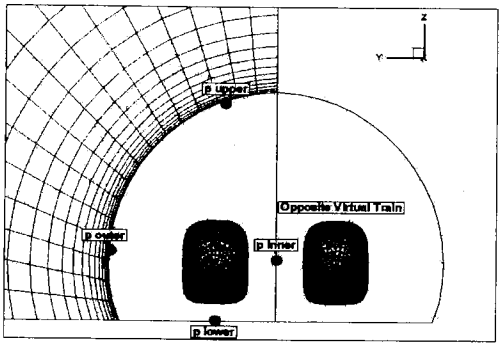

Fig. 6 Frontal view of grid system for crossing case and locations of tunnel wall pressure probes

Figure 8 (a)-(e) shows the aerodynamic load histories for all of the cases. The load variation with respect to time shows a similar pattern for all cases. Among aerodynamic forces, unsteady side force is the most significant and influential in determining the stability of crossing trains. When two trains are approaching each other, they start pushing each other away due to the high pressure region around the noses. So, the Cs curves have maximum positive peak around 1~2 second after the two noses meet depending on the nose length (Fig. 8). Following the progressive overlapping of two trains, low pressure at the inner side of the nose parts induces the attractive forces, and attractive force reach the maximum value when the two trains are located exactly side by side. Then, as they start parting away from the full overlapping position, the side force becomes repulsive again.

By comparing the cases of two (Fig 9(d)) and three cars (Fig 9(e)), it can be pointed out that there is no effect of the length of the train under our inviscid assumption. Peak values and overall trends of the curves of SFCO3 case are almost the same as those of the SFCO case except the elonga-

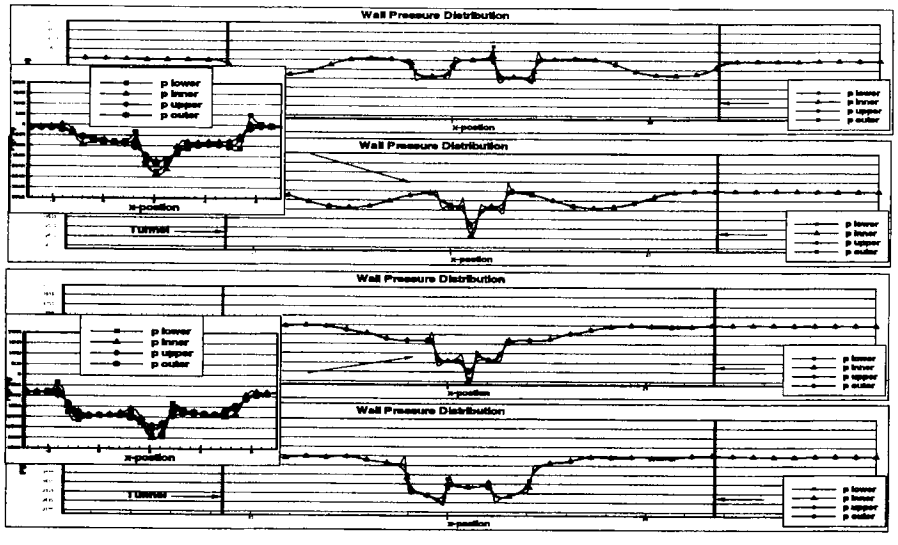

Fig. 7 Tunnel wall pressure distribution
(case SFCT-short frontal shape crossing in the Tunnel, t=110, 120, 130, 140)

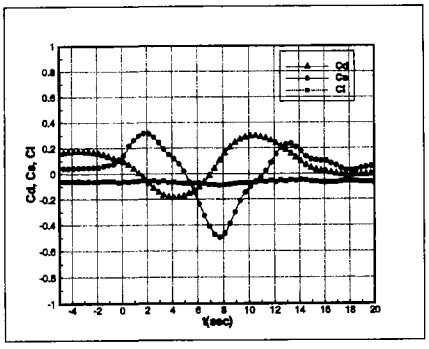

(a) Case LFCT-long frontal shape crossing in the tunnel

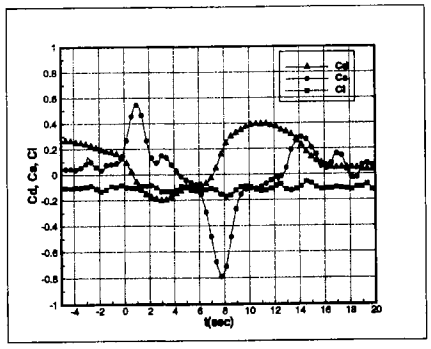

(b) Case SFCT-short frontal shape crossing in the tunnel

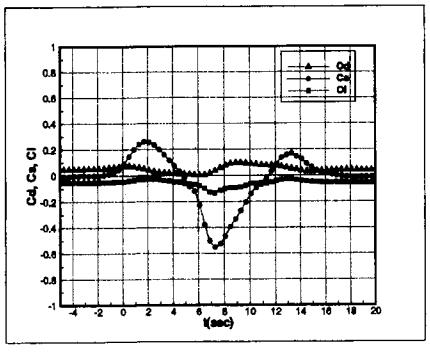

(c) Case LFCO-long frontal shape crossing at the open space

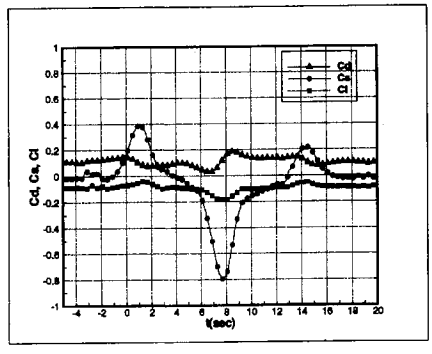

(d) Case SFCO-short frontal shape crossing at the open space

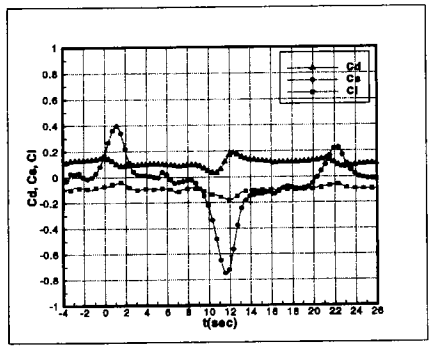

(e) Case SFCO3-short frontal shape crossing at the open space(3 Cars)

Fig. 8 Time history of aerodynamic force coefficients of train during crossing event

tion of the time between the peak values for side force.

Aerodynamic drag histories during the crossing show similar patterns for all cases, and they resemble point-symmetric curves about the point $t = 7.66$ for the case of two cars. When the fore nose is located at the side of the opposite train, the stagnation pressure of the nose is weakened by negative pressure field at the side and so the drag force is decreased. And, when the aft nose is positioned at the side of the opposite train, drag force is increased by the weakened base pressure.

Lift curves, which is not so important for the heavy ground vehicle, show negligible variations with small overall values. (Fig. 8) By comparing Fig. 8(a) and (b), Fig. 8(c) and (d), it

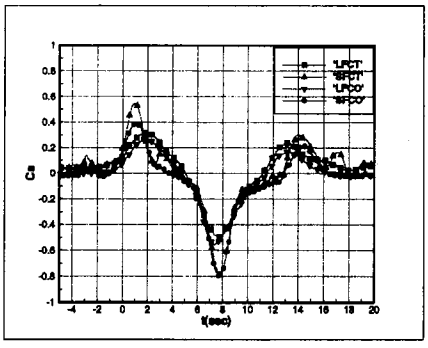

(a) Side force comparison

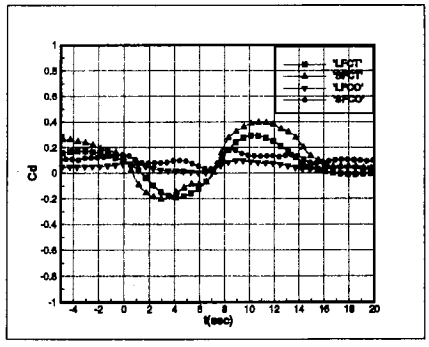

(b) Drag comparison

Fig. 9 Comparison of aerodynamic force coefficients of train during crossing for different nose shapes and locations

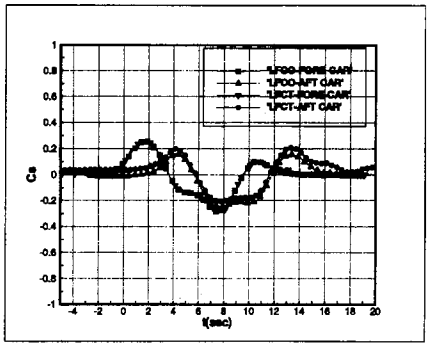

(a) Train of 2 cars

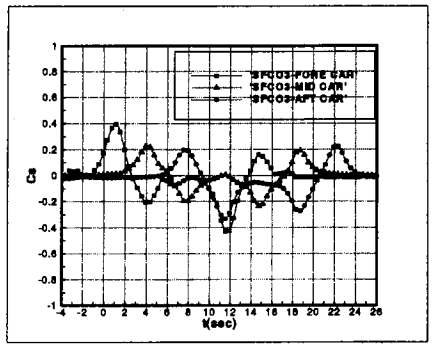

(b) Train of 3 cars

Fig. 10 Side force histories of each car for train consist of 2 and 3 cars

can be concluded that the time derivatives of the force coefficients are mainly affected by the nose shape of the train. This could be explained by the differences of the spatial distributions of flow properties that sweep the opposite train. Because the more the shape varies, the stiffer the flow properties are.

In Fig. 9, comparisons of side force coefficient(Cs) and drag coefficient(Cd) for 4 cases are given. Since the difference of pressure distribution between inner and outer side of the train surface during the crossing event is chiefly affected by the nose shape, it can be argued that the side force mainly depends upon the nose shape of train, not on the existence of tunnel as shown in Fig. 9(a).

From Fig. 9(b), it is shown that the strength of the drag variation is mainly affected by the location where the crossing event occurs. Cd curve's trend mainly depends on the location where the crossing events occur, not on the nose shape of the train, because the stagnation pressures of the two nose shapes are almost the same, and the flows remain 1-dimesional in the tunnel even during the crossing event.

In general, a train consists of cars connected by articulated connectors which permits yawing motions for each car. So the information about the side force distribution on the each car is indispensable data for design and analysis of bogie systems. Aerodynamic load histories can be taken for each car, if we perform the force integration over the separated parts, not over the whole surface (Fig. 10, Fig 11 and Fig 12). For the side forces (see Fig. 10), the curve for each car shows similar pattern and slightly different temporal distribution, which may result in severe snake-like motions of the train during the crossing. And, from Fig. 10(b), we can expect that mid-cars of the real train might undergo the same aer-

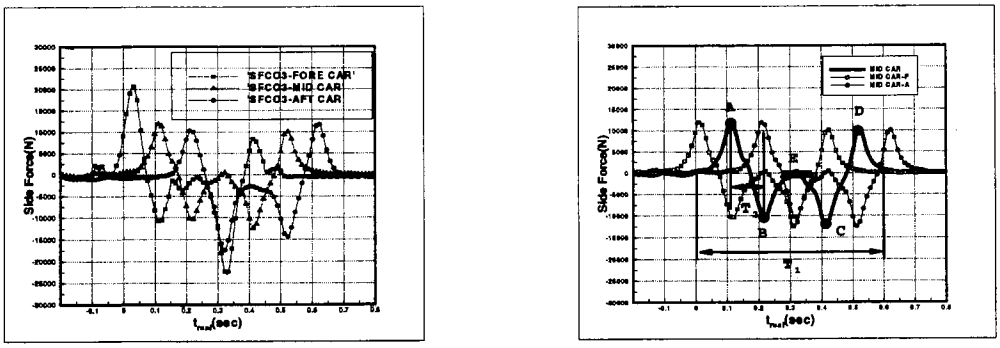

(a) Side force histories for 3 cars (b) Extension of side force History to multi-car train

Fig. 11 Side force histories in physical value for train consist of 3 cars running at 350km/h and extensions to multi-car train

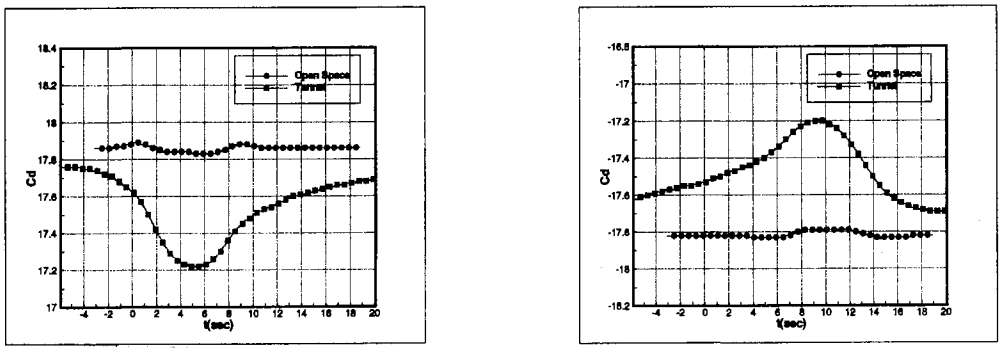

(a) Fore car (b) Aft car

Fig. 12 Drag histories of each car for 2-car train(long frontal shape cases)

odynamic load of the mid-car of the case. The aerodynamic side force histories on each car have two dramatic changing parts- 'push-pull part' when the fore nose of the opposite car sweeps the car, and 'pull-push part' when the aft nose of the opposite car sweeps it away. The time interval between the push-peak and the pull-peak is proportional to the nose length. The shorter the nose is, the narrower the interval is. And the time interval between the 2 'push-pull parts' is proportional to the train length. (see Fig. 8(e), Fig. 9(a) and Fig. 10(b))

The physical values of side forces with respect to the physical time are shown in Fig. 11(a). The force on the fore car changes from +20,000N to -10,000N in 0.1 second at the beginning of the crossing event, which can be treated as a great impulse on the nose. In order to extend the current results to a multi-car train without recomputation, a time scale should be defined as shown in Fig. 11(b). T_1 denotes the duration of the aerodynamic load variation which is proportional to the train length at the given speed of a train. T_2 denotes the duration of 'push-pull part' and 'pull-push part', which is proportional to the length of the nose and so to the length of one car approximately. For mid cars of a multi-car train, the 'push-pull part' (segment A-B) induced by the fore nose of the opposite train and the 'pull-push part'(segment C-D) would be repeated and the segment E would be increased proportional to T_1. Thus, simply, by shifting the curves about T2, the side force histories of fore and aft cars to a mid car can be guessed as shown in Fig. 11(b). The figure,shows that mid cars which are about 20 m long and running at 350 km/h might undergo the opposite directional side forces for two adjacent cars. (point A, B, C, D at the Fig. 11(b)).

As for the drag force, it is shown that fore car

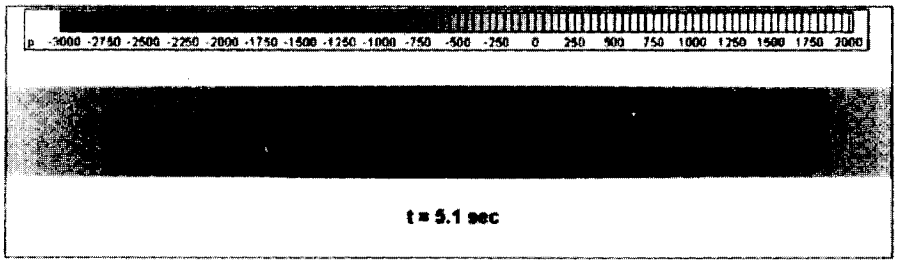

(a) In the tunnel

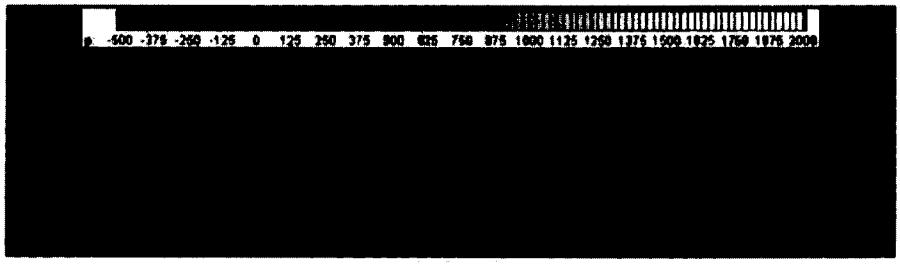

(b) At the open space

Fig. 13 Top view of pressure field of crossing event in tunnel and at open space for long frontal shape cases

and aft car undergoes temporally and directionally different drag during the crossing event and that drag variations are heavily dependent on the location as shown in Fig. 12. However, for a multi-car train, mid cars might have negligible drag variation.

In Fig. 13(a) and Fig. 13(b), the top views of the pressure fields ground and train for the LFCT and LFCO case are shown. As mentioned before, the strength of pressure variation for the LFCT case (inside a tunnel) is much higher than that for the LFCO case (open space). But, it is shown that nearly 1-dimensional pressure distributions in the tunnel are valid as is pointed before as the reason for the drag dependence on the locations(see Fig. 13(a)).

4. Concluding Remarks

To study unsteady aerodynamic loads on high speed trains when two trains are passing by each other, a three-dimensional inviscid numerical method, based on 3 types of domain decomposition technique, is developed and applied. Numerical simulations of trains passing by are conducted and discussions are given for five different cases using three basic parameters-nose shape, existence of tunnel, and train length.

From the results, some conclusions are drawn as follows ;

(1) Even during crossing event, one-dimensional pressure distribution along the tunnel is valid except in the vicinity of trains.

(2) Overall variations of side force and drag during the crossing are determined by the relative locations of the two passing trains. As the fore nose part passes by, 'push-pull' side force is induced, and as the aft part goes by, 'pull-push' side force is induced. Drag decreases when the fore nose is positioned at the side of the opposite train, and increases when the aft nose to located at the side.

(3) The side force variation depends mainly on the nose shape of a train, and the drag force variation depends mainly on the location where the crossing event occurs. Also, the sustained one-dimensionality in the tunnel even during the crossing procedure explains the different dependencies of the load histories.

(4) The current approach can give load data for each car of a multi-car train, and, thus, can be applied to multi-body dynamics of train.

Acknowledgement

The authors appreciate the financial supports rom the Government of Korea. This research is a ›artial result of 'Aerodynamic Design & Ana-yses of High-Speed Railway System.' This esearch is partly supported by iDOT ERC and ›K MECHA SNU.

References

Fujii, K., 1992, "Unified Zonal Method Based ›n the Fortified Solution Algorithm," ISAS Report No. 648.

Fujii, K. and Ogawa, T. 1995, "Aerodynamics ›f High Speed Trains Passing by Each Other," *Computers & Fluids*, Vol. 24, No. 8, pp. 897 ~908.

Holmes, B. S., Dias, J., Rifai, S. M., Buell, J. C., ohan, Z., Sassa, T. and Sato, T., 1999, "Solution ›f Train-Tunnel Entry Flow Using Parallel Computing," Computational Mechanics 23, pp. 24~129

Hwang, J. and Lee, D, 1998, "Development of Moving Grid Technique for Unsteady Analysis of High Speed Train," *Proceedings of the KSME '998 Spring Annual Meeting* B, pp. 607~610.

Hwang, J. and Lee, D, 1999, "Numerical Simu-ation of Flow field around High Speed Trains Passing by Each Other," *AIAA* Paper 99-3156.

Jameson, A., and Yoon, S., 1987, "Lower Upper Implicit Schemes with Multiple Grids for he Euler Equations," *AIAA Journal*, Vol. 25, ›p. 929~935.

Kim, H., 1997, "Aerodynamic Analysis of a Train Running in a Tunnel(II)-Aerodynamics of Two-Trains," *Transaction. of KSME*, pp. 983 ~995, No. 8, 21. 36.

Kwon, H., Lee, D., Lee. S., Kim. D. and Kang. S., 1998, "An Experimental Study on Propagation ›f Pressure Waves inside the Tunnel and Boom-ng Noise by a High-Speed Train," *Proceedings of the KSME 1998 Fall Annual Meeting* B, pp. 735~740.

Maeda, T. 1993, "Effect of Shape of Train Nose on Compression Wave Generated by Train Enter-ing Tunnel," *Proceedings of the International Conference on Speedup Technology for Railway and Maglev Vehicles*, PS3-8, pp. 315~319.

Mestreau, E., Lohner, R. and Aita, S., 1993, "TGV Tunnel Entry Simulations Using a Finite Element Code with Autometic Remeshing," *AIAA* 93-0890

Ogawa, T. and Fujii, K., 1994, "Numerical Simulation of Compressible Flows Induced by a Train Moving into a Tunnel," *Computational Fluid Dynamics Journal*, Vol. 3, No. 1.

Ogawa T. and Fujii, K., 1997, "Numerical Investigation of Three Dimensional Compressible Flows Induced by a Train Moving Into a Tun-nel," *Computers & Fluids*, Vol. 26, No. 6., pp. 565~585.

Peters, J. L., 1983, "Aerodynamics of Very High Speed Trains and Maglev Vehicles: State of the are and Future Potential," *Int. J. of Vehicle Design, Technological Advances in Vehicle Design Series*, SP3, Impact of Aerodynamics on Vehicle Design, pp. 308~341.

Rai, M. M. and Hessenius, K., 1986, "Three Dimensional Conservative Euler Computations Using Patched Grid System and Explicit Methods," *AIAA*-86-1081.

Roe, P. L., 1981, "Approximate Riemann Solvers, Parameter Vectors, and Difference Schemes," *Journal of Computational Physics*, Vol. 43, pp. 357~372.

Shimbo, Y., Hosaka, S., 1993, "Steady and Unsteady Pressure Measurement on High Speed Train," *Proceedings of the International Confer-ence on Speedup Technology for Railway and Maglev Vehicles*, PS3-14, pp. 341~346.

Steger, J. L., Dougherty, F. C. and Benek, J. A., 1983, "A Chimera Grid Scheme," *Advances in Grid Generation*, FED Vol. 5, ASME, edited by Ghia, K. N., New York, pp. 59~69.